Macromolecules

Article

pubs.acs.org/Macromolecules

Shedding Light on Structure–Property Relationships for Conjugated Microporous Polymers: The Importance of Rings and Strain

Martijn A. Zwijnenburg,[†,*] Ge Cheng,[‡] Tom O. McDonald,[‡] Kim. E. Jelfs,[‡] Jia-Xing Jiang,[‡,§] Shijie Ren,[‡,⊥] Tom Hasell,[‡] Frédéric Blanc,[∥] Andrew I. Cooper,[‡] and Dave J. Adams[‡,*]

[†]Department of Chemistry, University College London, 20 Gordon Street, London WC1H 0AJ, U.K.

[‡]Department of Chemistry and Centre for Materials Discovery, University of Liverpool, Crown Street, Liverpool, L69 7ZD, U.K.

[∥]Department of Chemistry and Stephenson Institute for Renewable Energy, University of Liverpool, Crown Street, Liverpool, L69 7ZD, U.K.

Supporting Information

ABSTRACT: The photophysical properties of insoluble porous pyrene networks, which are central to their function, differ strongly from those of analogous soluble linear and branched polymers and dendrimers. This can be rationalized by the presence of strained closed rings in the networks. A combined experimental and computational approach was used to obtain atomic scale insight into the structure of amorphous conjugated microporous polymers. The optical absorption and fluorescence spectra of a series of pyrene-based materials were compared with theoretical time-dependent density functional theory predictions for model clusters. Comparison of computation and experiment sheds light on the probable structural chromophores in the various materials.

INTRODUCTION

Conjugated microporous polymers (CMPs)[1−4] and related materials, such as covalent triazine-based frameworks (CTFs)[5,6] and porous aromatic frameworks (PAFs),[7,8] are a fascinating class of materials that can, in some cases, combine microporosity with useful physical properties that arise from their electronic conjugation.[9−12] CMPs typically comprise aromatic organic units covalently bonded to three or four neighboring units. Insoluble CMPs and related polymers, such as PAFs, hence have commonly been envisaged as extended 3- or 4-connected networks that contain rings but only a small number of end-groups.[7,13,14] If this picture is true, then CMPs, CTFs, PAFs, and their like, would be the closest organic polymer analogues of well-known inorganic materials such as boron nitride, zinc oxide, and (alumino)silicates, materials whose structures are also based on 3- or 4-connected networks.[15−17] Alternatively, however, these materials could also resemble highly branched polymers or dendrimers, which are tree-like molecules with a relatively large number of end-groups but, typically, no closed rings. Structural hypotheses and models[14] aside, it is essentially unknown if CMPs, CTFs, and PAFs can be best described as highly branched polymers or as extended networks, or even as small but insoluble oligomers, which might nonetheless exhibit permanent microporosity.[18] This uncertainty over structure mainly stems from the amorphous or poorly crystalline nature of the experimental samples, coupled with their total lack of solubility. However, the need to understand structure–property relationships is highlighted by the recent discovery of new porous materials, such as soluble, hyperbranched CMPs and porous dendrimers,[19] organic molecules of intrinsic microporosity,[18] and other discrete organic molecules[20−24] that can show high levels of microporosity in the amorphous, solid state. Hence, extended networks are not a prerequisite for microporosity, and network structures cannot simply be assumed because a given material is microporous, particularly since typical CMP structures, which lack any deliberate solubilizing functionality, would be expected to become insoluble at quite modest molecular weights. It is important, therefore, that methods are developed to elucidate the molecular structures of CMPs, rather than simply inferring them based upon observations of permanent microporosity.

The experimental determination of the number of end-groups, for example by solid-state NMR, should in principle allow us to differentiate between, e.g., dendrimers and highly extended condensed networks. In practice, however, this is difficult because side-reactions might cleave such end-groups, making them invisible to NMR and artificially lowering the end-group-to-molecular unit ratio. For example, in nickel-coupled Yamamoto polymerizations of tetrahedral aryl halides,[7,8] it is possible that halogen end groups might be removed by metal-catalyzed dehalogenation. Additionally, entrained gases, physisorbed water vapor, or residual catalyst can all lead to difficulties in the precise determination of end-group concentration by elemental analysis.

In this study, we take an alternative approach and focus on optical absorption and fluorescence spectra for CMPs as a

Received: June 25, 2013
Revised: August 28, 2013
Published: September 16, 2013

handle on their molecular structure. We believe that this is a useful strategy, because the electronic properties of CMPs are in any case central to many of their most interesting applications.[12] We demonstrate that the optical properties of CMPs give a unique insight into the structural elements present in the CMP. Furthermore, we show that this structural knowledge can also be exploited in terms of engineering the optical properties of CMPs and related compounds. We concentrate here on CMPs based on the polymerization of pyrene monomers,[4,19] but the general approach should be broadly applicable to other CMPs and compounds such as CTFs and PAFs.

EXPERIMENTAL SECTION

Materials and Nonoptical Characterization. All reagents and solvents were purchased from Aldrich. Reactions were carried out under a nitrogen atmosphere. Thin layer chromatography (TLC) was performed using precoated aluminum sheets with silica gel 60 F254 (Merck) and visualized by UV light (λ = 254 or 280 nm). Merck silica gel 60 was used for column chromatography. Solution ^{1}H NMR spectra were collected on a Bruker UXNMR/XWIN-NMR 400 MHz spectrometer while the solid-state ^{13}C NMR spectrum for the ECMP was collected a 9.4 T Bruker DSX NMR 400 MHz spectrometer equipped with a 4 mm HXY triple-resonance MAS probe (in double-resonance mode). FTIR Spectra for the ECMP and its precursors were collected on a Bruker Tensor 27 spectrometer equipped with a Specac attenuated total reflectance module. Gel permeation chromatography (GPC) utilized a LC 1120 HPLC pump, a PL-ELS 1000 Evaporative Light Scattering Detector, a PL gel 5 mm MIXED-C GPC column and Midas autosampler (Polymer Laboratories Ltd. U.K.). THF was used as the eluent with flow rate of 1.00 mL/min at 40 °C and polystyrene as the standard. Full synthetic details and nonoptical characterization results are given in section ESI-1 of the Supporting Information.

Optical Characterization. Solution measurements for the soluble materials were obtained at 0.04 and 0.004 mg/mL (1,3-linear pyrene polymer and SCMP) and 1.5 mg/mL (Py(5) dendrimer) respectively in DCM. For the same soluble materials thin film samples were prepared by dissolving 20 mg (1,3-linear pyrene polymer and SCMP) or 6 mg (Py(5) dendrimer) of the compounds in 1 mL of DCM, after which the resulting solution was added to a quartz cuvette held at an angle and left overnight to evaporate. The resulting film on the inside of the cuvette provided a range of film thicknesses for analysis (thickest at the bottom of the cuvette). Measurements for solid-state powders were obtained by grinding the sample with KBr. The resulting powder was approximately 99% KBr (by mass).

UV−Vis Spectroscopy. UV−vis spectra were obtained using a Shimadzu UV-2550 UV−vis spectrophotometer running the UVProbe software, version 2.34. All spectra were obtained as absorbance measurements from 200−800 nm, with scan speed set to fast and using a slit width of 5 nm. Film and solution samples were measured in a quartz cuvette as a transmission measurement. Solid powdered samples were analyzed using the ISR-2200 integrating sphere attachment with a quartz solid sample holder as diffuse reflection measurement.

Fluorimetry. Emission and excitation spectra were obtained on a Shimadzu RF-5301PC spectrofluorophotometer running RFPC software, version 2.04. Spectra were obtained using a fast scan speed and with sensitivity set to high. Slit widths were adjusted so as to maximize the signal-to-noise for each sample. Solution samples were analyzed in a quartz cuvette with the standard cell holder attachment. Film samples were analyzed adhered to the wall of a quartz cuvette placed in the solid (powder) holder attachment. Powder samples were analyzed in a quartz solid sample holder held in the solid (powder) sample holder attachment. Data was exported to Excel for further processing, and second order diffraction peaks of the excitation wavelength were manually removed from the spectra and the long wavelength baseline set to zero.

Computational Methods. The excited state properties of pyrene oligomer model clusters were calculated using a six-step approach. First, for each cluster model we performed a conformer search using the OPLS-AA forcefield[25] and the low-mode sampling[26] algorithm as implemented in MacroModel 9.3 (for more details about the conformer search see section ESI-2 of the Supporting Information) Second, the ground state singlet (S_0) geometries of the low-energy conformers found in the conformer search were optimized using ground state density functional theory (DFT) calculations. Third, where possible, the harmonic frequencies at these optimized S_0 geometries were calculated using the same DFT setup to verify that the optimized structures correspond to proper minima on the S_0 energy surface. Fourth, the excitations at the optimized S_0 geometry were calculated using time-dependent density functional theory (TD-DFT). Fifth, the lowest singlet excited state of each oligomer was relaxed using TD-DFT,[27,28] to obtain its minimum energy geometry. Finally, frequency calculations on the excited state minima were performed for selected oligomers to verify that they correspond to proper minima on the TD-DFT excited state energy surface. For the DFT/TD-DFT calculations mainly the range-separated hybrid XC-functional CAM-B3LYP[29] was used and in some selected cases also the plain hybrid XC-functional B3LYP[30] (mainly to study the ground state energetics), where for all excitation calculations the Tamm−Dancoff approximation to TD-DFT was employed. All the DFT/TD-DFT calculations employing the CAM-B3LYP XC-functional used a combination of NWChem 6.0[31] (vertical excitation energies) and GAMESS-US[32] version 1 October 2010 R1 (vertical excitation energies, excited state optimizations) and the 6-31G** split-valence basis-set.[33] All the DFT calculations employing the B3LYP XC-functional were performed using the Turbomole 6.3.1 code,[34,35] and employed the double-ζ DZP[36] basis-set.

RESULTS AND DISCUSSION

The pyrene-based CMP network (Scheme 1b) obtained by homopolymerization of 1,3,6,8-tetrabromopyrene (see Scheme 1a for atom labeling of pyrene) has a reported Brunauer−Emmett−Teller (BET) surface area of 1508 m^2/g and is highly fluorescent.[4]

The pyrene-based CMP network is a member of a broad family of related pyrene-based polymers and oligomers reported previously in the literature. This family of structures includes a 1,3-linear polymer based on the Yamamoto coupling of 1,3-dibromo-7-*tert*-butylpyrene (Scheme 1c),[37] first-and second-generation dendrimers (Py(5) and Py(17), respectively) based on pyrene coupled via the 1,3,6 and 8 positions (Scheme 1e),[38] and a branched statistical copolymer of 1,3,6,8-tetrabromopyrene and 1,3-dibromo-7-*tert*-butylpyrene.[19] The latter copolymer combines porosity with solubility in selected solvents, and we hence refer to this as a soluble CMP or "SCMP". Finally, we note that the synthesis of a linear polymer, obtained through coupling of pyrene via its 2 and 7 positions, has also been reported.[39] However, this material is less closely related to our pyrene CMP[4] than other pyrene polymers and oligomers because the pyrene monomer is linked through positions other than 1, 3, 6, and/or 8, and it has very bulky aryl substituents on the 4,5,9 and 10 positions. As such, we do not discuss this material here. Hence, we have considered four possible basic architectures: a linear soluble pyrene polymer, perfectly branched, soluble pyrene dendrimers, a branched soluble pyrene polymer (the SCMP), and a branched pyrene CMP "network".

As a first step in understanding the structure of the pyrene-based CMP network, we prepared samples of the insoluble CMP network,[4] and the soluble 1,3-linear polymer,[37] Py(5) first-generation dendrimer,[38] and SCMP.[19] We also synthesized a novel copolymer (ECMP, for 'expanded-CMP') via the cross-

dx.doi.org/10.1021/ma401311s | Macromolecules 2013, 46, 7696−7704

Scheme 1. Structure of (a) Pyrene with Positional Numbering System; (b) Idealized Structure of Polypyrene CMP Network; (c) 1,3-Linear Pyrene Polymer; (d) 1,8-Linear Pyrene Polymer; (e) Py(5) Dendrimer[a]

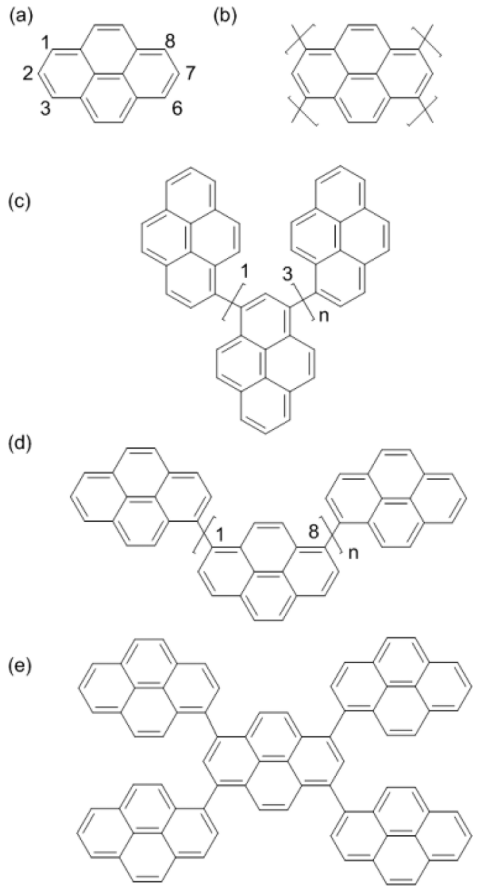

[a]Note, solubilizing *tert*-butyl groups on the 7-position of structures c and e have been removed for clarity.

coupling of 1,3,6,8-tetrabromopyrene and 1,3-diboronic ester-7-*tert*-butylpyrene (Scheme 2). Unlike the SCMP, which is a

Scheme 2. Synthesis of an "Expanded" Pyrene CMP, ECMP

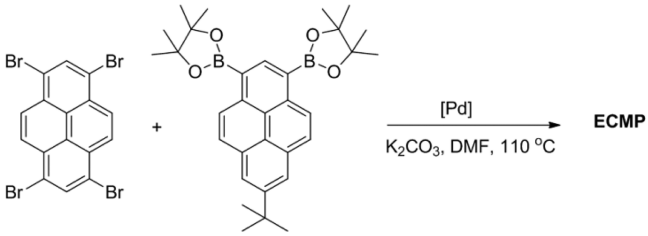

statistical copolymer based on similar monomers and where, for example, two 1,3-substituted pyrene monomers (bifunctional units) might link directly to each other, the ECMP will have an alternating copolymer structure, where 1,3,6,8- substituted pyrene monomers (tetrafunctional units) are only linked to 1,3-substituted pyrene monomers and vice versa. A further immediate difference between ECMP and SCMP is the lack of solubility for ECMP: by contrast, the analogous SCMP statistical copolymer is soluble in a range of common solvents.[19] Full synthetic details and characterization data are available in the Supporting Information for all these materials (section ESI-1).

We next measured the absorption and fluorescence spectra for these samples in solution, where possible, as a thin film cast from solution (again, where possible), and as a powder mixed with KBr (the only option for the insoluble CMP and ECMP). These measurements were compared with those reported previously in the literature for the 1,3-linear polymer material (solutions and thin films),[37] for the Py(5) material (solution),[38] for the SCMP material (in solution),[19] and for the insoluble CMP (powder).[4] This is the first systematic comparison of the solid-state and solution phase spectra of these materials. We concentrate here mostly on the fluorescence spectra, partly because the powder absorption spectra appeared significantly broadened relative to thin films, possibly due to scattering effects related to the polymer particle size distribution (there is also a small red shift in the fluorescence peak position between the thin film and powder spectra, e.g., 10 nm in the case of 1,3-linear polymer material, possibly also due to scattering, but with no real effect on the spectrum shape, for more details see section ESI-3 of the Supporting Information). Moreover, in the case of a structurally heterogeneous material, such as the insoluble pyrene CMP/ECMP and SCMP are likely to be, the absorption spectrum will be a convolution of the absorption spectra of a range of different structural elements (chromophores), all of which displaying vibrational broadening. As a result, the absorption spectra are harder to interpret in simple terms.

Figure 1 shows the normalized experimental fluorescence spectra for the various powder samples. The insoluble CMP 'network' fluorescence spectrum is significantly red-shifted compared to the other materials, with the wavelength of the fluorescence maximum increasing as follows: 1,3-linear polymer (479 nm, 2.6 eV) < Py(5) dendrimer (501 nm, 2.5 eV) < SCMP (526 nm, 2.4 eV) < ECMP (530 nm, 2.3 eV) < insoluble CMP (618 nm, 2.0 eV). It is apparent that the chromophores responsible for fluorescence in the CMP network and ECMP are quite distinct from those from the fluorescent chromophores in the 1,3-linear polymer and the Py(5) dendrimer. It is also clear that the insoluble CMP fluorescence chromophore is absent in the analogous soluble polymeric materials—most obviously in the 1,3-linear polymer, which does not fluoresce at all in this wavelength range. These fluorescence spectra demonstrate that at least part of the insoluble pyrene CMP network and the ECMP structures are fundamentally different in character from those of the 1,3-linear pyrene polymer and the Py(5) dendrimer.

We suggest that it is unlikely that these profound differences in the fluorescence spectra can be ascribed simply to the size or effective molecular weight of the conjugated pyrene system. For example, from the solution data of Figueira-Duarte et al.,[38] we know that the difference in fluorescence energy of the two dendrimers Py(5) and Py(17) is less than 0.1 eV while the system more than triples in size. Similarly, we know, based on solution data for the 1,3-linear pyrene dimer and trimer oligomers and the 1,3-linear pyrene polymer, that the fluorescence energy is effectively converged with the pyrene dimer.[37,38] It is thus unlikely that simply increasing the number of conjugated units can explain the large observed red shift in fluorescence for the insoluble pyrene CMP, or indeed even the much smaller red shift observed for ECMP. We also believe that these differences do not arise from agglomeration related effects. We studied two different SCMP samples; one sample

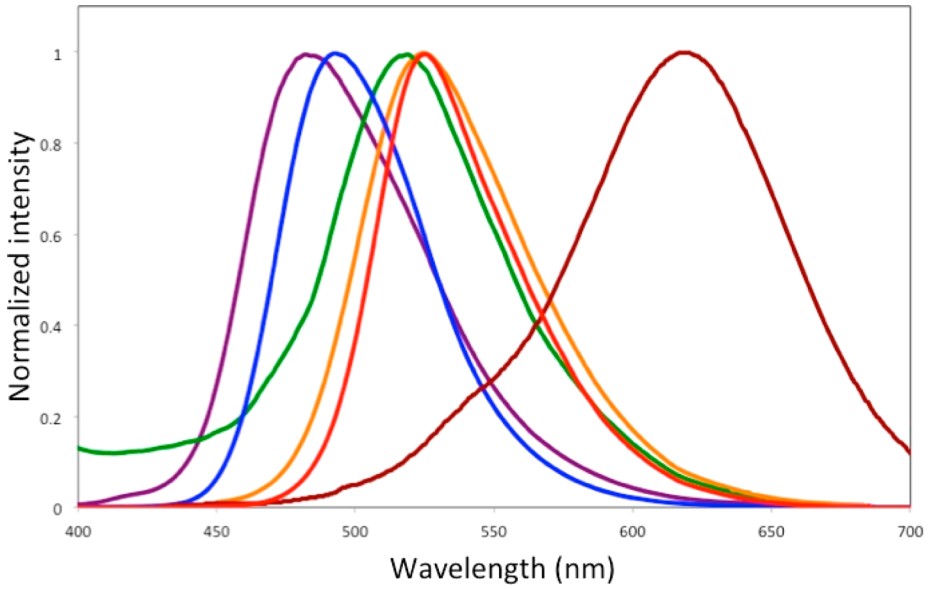

Figure 1. Experimental fluorescence spectra for the 1,3-linear pyrene polymer (purple), Py(5) pyrene dendrimer (blue), SCMP (cast film green, precipitated film orange), ECMP (light red) and CMP (dark red), clearly showing the red shift in the spectra. In all cases the excitation wavelength, λ_{ex}, lay between 350 and 360 nm.

obtained through precipitation with an antisolvent (orange line in Figure 1) and one obtained through slow evaporation of the solvent (green line in Figure 1). Both samples differ strongly in density and porosity to gases (precipitated materials have much higher porosity than cast materials, where the precipitated material absorbs nitrogen in micropores while the cast material is impervious to nitrogen)[19] and thus probably in degree of agglomeration. The difference in the position of the peak maximum for cast and precipitated SCMP (8 nm, 0.03 eV) is, however, small, especially in comparison with the red shift between the 1,3-linear polymer and the pyrene CMP (see section ESI-3, Supporting Information).

A comparison of the experimental solid-state (powder) absorption spectra (see Figure S3, section ESI-3 of the Supporting Information), while complicated somewhat by the peak-broadening problems discussed above, also suggests that the bulk of the CMP and ECMP structure are different from that of the 1,3-linear pyrene polymer and the pyrene Py(5) dendrimer. Not only are the first absorption maxima of the CMP (417 nm, 3.0 eV) and the ECMP (430 nm, 2.9 eV) red-shifted compared to both the 1,3-linear polymer (370 nm, 3.4 eV) and Py(5) dendrimer (397 nm, 3.1 eV), but the CMP and ECMP peak are also much broader. The dendrimer absorption spectrum reaches 25% of the maximum intensity of the first peak at 477 nm (2.6 eV, i.e. 0.5 eV below the peak maximum) while the absorption spectrum of the CMP reaches the same 25% already at 605 nm (2.0 eV, i.e. 1.0 eV below the peak maximum). Part of this ∼0.5 eV of extra broadening of the CMP absorption spectrum might be due to a difference in the inherent vibrational broadening of the CMP and the dendrimer and/or a difference in the scattering-related broadening highlighted above. However, the extent of the broadening also suggest, like for the fluorescence data, the presence of chromophores in the insoluble pyrene CMP and ECMP that absorb at wavelengths longer than the peak maximum (i.e., λ_{abs} > 417 nm and >430 nm respectively)—that is, a much greater red shift than suggested by the peak maximum alone. Again, solution data appear to rule out an explanation for this red shift based on an increased conjugation length. In summary, both solid-state absorption and fluorescence spectra suggest that a significant component of the insoluble pyrene CMP and ECMP are structurally different to both the 1,3-linear polymer and the Py(5)/Py(17) dendrimer.

We therefore decided to use computational chemistry calculations on cluster models of the polymer as a means to rationalize these qualitative observations and to elucidate the type of chromophore that might explain the large observed spectral red shift in the pyrene CMP and ECMP networks. The various cluster models that we investigated included fragments of linear polymers, fragments of dendrimers, and closed pyrene rings comprising between three and six pyrene units. We predicted the absorption and fluorescence spectra for the various cluster models and, where relevant, considered a range of conformers. In keeping with Kasha's rule,[40] we assumed in the fluorescence calculations that transitions from higher singlet excited states (e.g., S2) to S1 are so fast that fluorescence occurs in appreciable yield only from the latter S1 state.

We first focused on the materials for which we have good knowledge of the molecular topology: that is, the 1,3-linear pyrene polymer and the Py(5) dendrimer. In previous work,[41] we demonstrated that TD-CAM-B3LYP gives a good match to experimental absorption and fluorescence spectra of linear 1,3-oligomers and 1,3-linear polymer in solution after applying a rigid downward shift to account for the effect of environment (i.e., in this case, solvent) and an inherent bias of the CAM-B3LYP density functional that results in the general over-estimation of excitation energies. Moreover, we showed that the spectral features converge rapidly with oligomer length, and that chains of six pyrene units (in the case of absorption) and just two pyrene units (in the case of fluorescence) give peak maxima predictions that are close to those of an infinite polymer. Also, it was found that the *tert*-butyl groups could be omitted without significantly changing the results.[41] Since we are interested here in solid-state versions of the various polymers, we repeated this earlier analysis for both the 1,3-linear pyrene polymer and the Py(5) dendrimer (Scheme 1c

dx.doi.org/10.1021/ma401311s | *Macromolecules* 2013, 46, 7696−7704

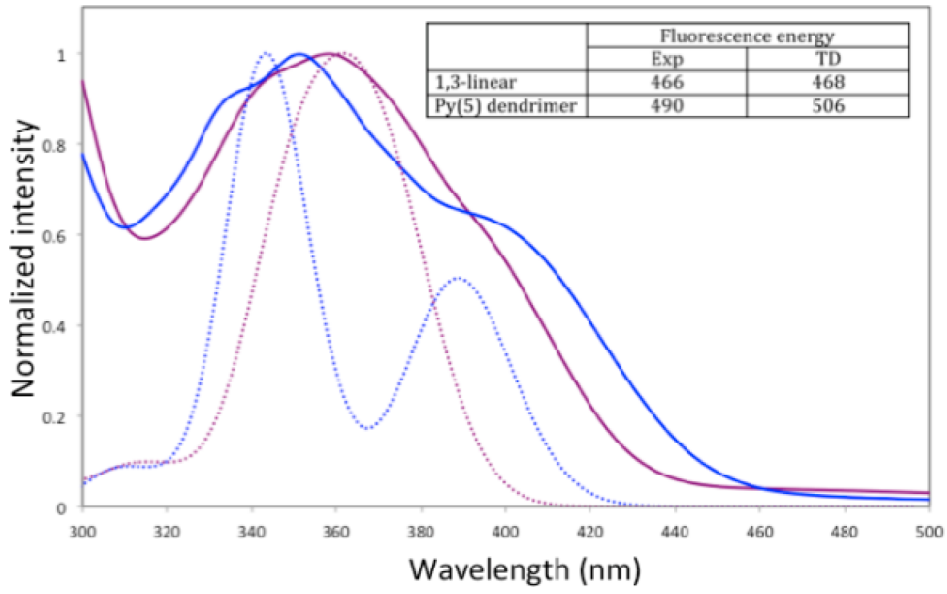

Figure 2. Comparison of the experimental (solid lines) and TD-CAM-B3LYP predicted absorption (dashed lines) and fluorescence (insert) spectra of 1,3-linear pyrene polymer (purple) and the Py(5) pyrene dendrimer (blue).

and 1e, respectively), and compared TD-CAM-B3LYP predictions with experimental data (Figures S4 and S7 in section ESI-3 of the Supporting Information) for thin films. We focus on films for these solution-processable materials, rather than powders, because the thin film data have, as discussed above, a much better resolution for the absorption spectra. We found that TD-CAM-B3LYP correctly predicts the relative ordering of the first absorption peak maximum of the 1,3-linear polymer versus the first absorption peak maximum and shoulder of the Py(5) dendrimer, and also the relative positions of the fluorescence peak maxima for both materials. For thin film data, application of a rigid downward shift of 0.5 eV to the TD-CAM-B3LYP predictions resulted in a good absolute match between the predicted and observed positions of spectral features (see Figure 2), and hence, all computational spectroscopic results hereafter include the same absolute shift. As the absorption and fluorescence maxima of the powder samples are further red-shifted by ~0.1 eV relative to those of thin-film samples (see discussion above and section ESI-3 of the Supporting Information), this may mean that our calculated corrected spectra need to be further red-shifted by a similar amount when comparing to powder spectra.

For systems such as the 1,3-linear pyrene polymer and the Py(5) dendrimer there are only a limited number of possible conformers that all lie relatively close in energy. Moreover, these conformers are generally predicted to have very similar optical properties. For example, the lowest excitation energy of the Py(5) dendrimer varies by less than 0.05 eV between the five different conformers (see also Figure S9 in section ESI-4 of the Supporting Information for an example of the effect of oligomers in the case of 1,3-linear pyrene oligomers).

Next, we considered an alternative chromophore structure that is strongly related to the 1,3-linear pyrene polymer but which has not, to our knowledge, been prepared experimentally: the 1,8-linear polymer (see Scheme 1d). Nonetheless, this substitution pattern is (theoretically) possible, and would result from the "linear" Yamamoto coupling of 1,3,6,8-tetrabromopyrene, followed by debromination from the remaining two brominated positions per pyrene unit. 1,3,6,8-Tetrabromopyrene does not have a C4 axis, but only a C2 axis perpendicular to the plain of the ring; that is, it is 'rectangular' rather than "square", Scheme 1). Hence, the relative orientation of the pyrene units in the chain results in the 1,3- and 1,8-linear pyrene polymers being structurally different and having different optical properties. The 1,8-oligomers, and by extrapolation the 1,8-linear polymer, is predicted to have spectral features that are slightly red-shifted compared to the 1,3-linear polymer, but rather similar to the dendrimer; fluorescence at 500 nm (2.5 eV) and two strong absorption features at 400 nm (3.1 eV) and 375 nm (3.3 eV), respectively (see also Table 1 and Figure S9 in section ESI-4, Supporting Information). 1,8-Linear polymers and oligomers thus do not

Table 1. Position of the First Absorption and Fluorescence Peaks Predicted for the Different Chromophores.[a]

	absorption	fluorescence
1,3-linear polymer	3.4	2.6
1,8-linear polymer	3.3 (3.1)	2.5
dendrimer	3.6 (3.2)	2.4
3SSS	2.3	1.5
3LLL	2.4	1.8
4SSSS	2.8–**3.3**	1.9–**2.8**
4LLLL	2.6–**3.1**	2.1–**2.5**
4LSLS	2.6–**3.0**	2.1–**2.4**
5SSSSS	3.0	2.6
5LLLLL	2.7–**3.1**	2.1–**2.5**
5LSLSL	3.0–**3.1**	2.4–**2.5**
6SSSSSS	3.3	2.7
6LLLLLL	3.1	2.6
6LSLSLS	3.5	3.2

[a] All values are in eV and, as discussed in the text, rigidly shifted downwards by 0.5 eV. For all 4- and 5-ring chromophores, the observed spread in excitation energies for the different conformers is presented with the value for the lowest energy conformer in bold. For the linear polymers and dendrimers, the position of likely (lower intensity) shoulder peaks is given in parentheses.

dx.doi.org/10.1021/ma401311s | *Macromolecules* 2013, 46, 7696–7704

appear to make good candidates for the red-shifted spectral features in the CMP and ECMP.

Having considered linear polymers and dendrimers, we next considered possible cluster fragments of extended networks containing rings. The possible existence of rings, or "loops", has been invoked previously in a structural model for PAF-1 based on isomorphous replacement in an amorphous silica model.[14] Here, we focused on rings consisting of three to six pyrene units. It is known from topological considerations that every 4-connected network will have at least a certain fraction of rings in this size-range.[15,16,42] We also considered different types of rings for each ring-size. For the reasons outlined above, the orientation of the pyrene units in the ring lead to structurally different rings. The long sides (i.e., 1−8 or 3−6) and short sides (i.e., 1−3 or 6−8) of the pyrene units give rise to L(ong) and S(hort) edges, respectively. These L and S edges can combine into rings made of either just one type of edge (A) or a combination of both types of edges (B). Henceforth, we label such rings by the number of pyrene units in the ring, followed by the orientation of the edges. For example, the two possible A-type rings formed from four pyrene units are labeled 4LLLL and 4SSSS, respectively, while an example of a possible B-type ring is 4LSLS (see also Figure 3). Because every pyrene unit has two L and two S sides, a mixture of different ring configurations is always expected to occur in the extended material.

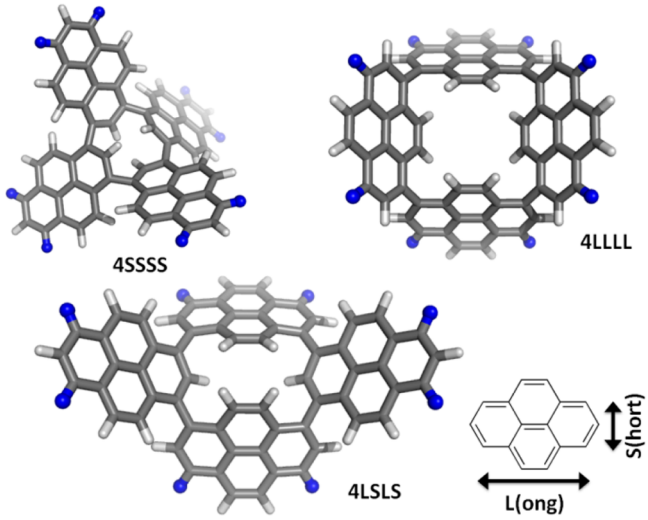

Figure 3. DFT-optimized lowest energy configurations of 4LLLL, 4SSSS and 4LSLS rings (atoms represented as blue spheres indicate where the rings would connect to the rest of the amorphous pyrene network in the pyrene CMP/ECMP).

We also considered a number of distinct conformers for the 4- and 5-rings (typically 2 or 3, distinguished from each other by a superscript number at the end of the ring label: that is, $4LLLL^1$ for the lowest energy, or first, conformer of the 4LLLL ring, $4LLLL^2$ for the second most stable, etc. This was done to sample the possible conformations rings could have when they form part of an extended framework. Competing bonding requirements make it unlikely that in an extended material all rings would be in their lowest energy conformation. Figure 4 shows the $4SSSS^2$ and $4SSSS^3$ conformers ($4SSSS^1$ is shown in Figure 3) and illustrates that the difference between different conformers lies in the relative orientation of the different pyrene units (e.g relative to the plane of the ring up−down−

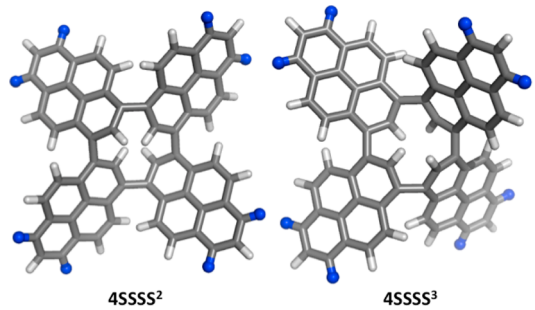

Figure 4. DFT-optimized lowest energy configurations of the $4SSSS^2$ and $4SSSS^3$ conformers ($4SSSS^1$ shown in Figure 3).

up−down for $4SSSS^1$, flat-down-flat-up for $4SSSS^2$ and flat-up−down−down for $4SSSS^3$).

Table 1 summarizes our predictions for the location of the fluorescence and the first absorption peaks for the different rings (see Table S2 in section ESI-5 (Supporting Information) for the unshifted energies). Focusing first on the lowest energy conformers of each ring type, we observe that the lowest absorption and fluorescence peak of the 3SSS and 3LLL rings lie at significantly lower energy (and hence longer wavelength) than those predicted for the different linear polymer and dendrimer cluster models. In the case of the other ring types, the position of the lowest absorption and fluorescence peak is, however, generally very similar to those predicted for the structurally related polymers (i.e., the 1,3-linear polymer for the pure S rings and the 1,8-linear polymer for the pure L rings). That said, the energy of the lowest absorption peak is always slightly lower than that of the corresponding linear oligomer of the same length (i.e., 4SSSS vs the 1,3-coupled tetramer, see Figure S9 in section ESI-4, Supporting Information). The only exception is the lowest absorption peak (but not fluorescence peak) of the 5SSSSS ring, which is red-shifted by 0.4 eV compared with both the 1,3-coupled linear pentamer and the 1,3-linear polymer. Surprisingly, the lowest energy conformers of most rings built from more than three pyrene units thus show generally only minor evidence of ring-strain in their spectra. The higher energy conformers of the rings (lying ∼20−60 kJ/(mol pyrene) higher in energy), however, show a different picture. For these conformers, the position of the first absorption and fluorescence peaks are significantly red-shifted compared with the linear polymer and dendrimers. More specifically, for each ring-size, we found that the more strained the conformer—that is, the higher its energy with respect to the lowest energy conformer—the lower in energy and higher in wavelength the fluorescence peak and first absorption peak are predicted to lie. Clearly, then, the presence of such strained rings could give rise to a red shift in both the fluorescence and absorption spectra of CMP and ECMP networks.

For the CMP network specifically, the measured fluorescence spectrum fits well with the fluorescence energies predicted for the more strained 4- and 5-rings, and suggests that such rings might be the chromophores responsible for the large red shift in the CMP fluorescence. Regarding the absorption spectrum, this again will be a convolution of the absorption spectra of a range of different chromophores. In principle, the red shift and broadening of the CMP absorption spectrum could be explained by a combination of different ring-sizes, configurations, and conformations as present in an amorphous network. We propose that the bulk of the rings would be moderately strained 4-, 5-, and 6-rings, and that these

dx.doi.org/10.1021/ma401311s | Macromolecules 2013, 46, 7696−7704

chromphores are responsible for the shift of the first absorption maximum to 3.0 eV (310 nm). A smaller fraction of more strained rings could account for the chromophores responsible for broadening the CMP absorption spectrum to even longer wavelengths, the most strained of which would be the strained 4- and 5-ring chromophores responsible for the fluorescence. In line with this evidence of rings in CMPs, energetic estimates (discussed in the Supporting Information, section ESI-6) suggest that the formation of rings, even small or strained ones, is energetically feasible during the kinetically driven CMP synthesis which involves irreversible bond-formation, especially when one takes into account that some of the polycondensation might take place after phase separation within the porous, precipitated network phase. Overall, we thus believe that a structural model of the CMP should contain the above-described rings (and indeed our previous preliminary model of the pyrene CMP contained rings[4]).

The likely microscopic link between strain and the spectroscopic red shift are the pyrene−pyrene torsion angles. Smaller torsion angles—that is, flatter structures—are expected to result in increased overlap between the π-systems on adjacent pyrene units and hence enhanced conjugation, which would explain, for example, the observed red shift in the absorption energies. Indeed we find that the strained rings that display a large red shift have considerably smaller average torsion angles than those of their chain counterparts; e.g., 42° for $3LLL^1$ and 46° for $4SSSS^2$ compared with ∼70° for long 1,3- and 1.8-linear chains. Likewise, those rings that have a similar absorption on-set as the linear-polymers also have average torsion angle comparable to that of linear chains; e.g., 67° for $4SSSS^1$. See Supporting Information, section ESI-5, for more information about the torsion angle distributions of the rings. Small torsion angles, in the absence of rings, could also result in a significant red shift (at least in the case of the absorption spectrum, see for example data for linear chains in Figure S10 in section ESI-7 of the Supporting Information). However, it is difficult to envisage where the strain required for the formation of these small torsion angles should originate from, if not from the presence of rings.

A comparison of the data in Table 1 and the experimental fluorescence spectrum of the pyrene CMP in Figure 1 suggests that fluorescence occurs from only the most strained subset of chromophores and not from the less strained chromophores (though there might be a shoulder at 540 nm, 2.8 eV), despite the fact the less strained chromophores do appear to contribute to the absorption spectrum. Our calculations, discussed in more detail in the Supporting Information (section ESI-8), suggest that this might be because an excited ring-based system can lower its energy significantly by moving the excited state from larger rings to smaller rings (e.g., 5LLLLL* + 4LLLL → 5LLLLL + 4LLLL*, where the asterisk denotes the ring upon which the excited state is localized) and, for a given ring-size, from a less strained conformer to a more strained conformer (e.g., $4LLLL^1$* + $4LLLL^2$ → $4LLLL^1$ + $4LLLL^2$*). Assuming that excited state transport is generally fast relative to excited state relaxation, then excited state relaxation and fluorescence would indeed only occur at the most strained chromophores in the material, even though all chromophores to some extent contribute to absorption. The possible shoulder at 540 nm (in the range where fluorescence is predicted to occur from unstrained 4SSSS- and 6SSSSSS/LLLLLL-rings) might then be indicative of those cases where excited state transport is too slow and/or strained rings too far away from the absorption chromophore for the excited state to reach the most strained ring before fluorescence. In this scenario, the appearance of multiple fluorescence peaks or shoulders could potentially be a marker for material heterogeneity (e.g., the spatial distribution of small rings or linear fragments, see below, over the bulk of the material).

For the ECMP, the measured fluorescence spectrum matches the fluorescence energies predicted for moderately strained 4SSSS and 4LSLS rings (configurations by definition including *short* edges, see Figure 3, in-line with the fact that the bifunctional 1,3-pyrene units, by definition, will be incorporated "*short*" in any ring that is formed. Thus, perhaps counter-intuitively, expanding the CMP by inserting bifunctional units between the tetrafunctional units does not seems to lead to an apparent change in the size of the smallest ring in the network, but only the degree of strain that these small rings are under. The lower strain could be either (i) the direct result of having bifunctional units in the ring that are relatively free to move, since they do not form part of any other rings, or (ii) an environmental effect due to other rings surrounding the small ring being larger than in the related CMP. The fact that no shift in the size of the smallest ring is observed fits with the idea that the pyrene ECMP and CMP are kinetic and not thermodynamic products.

A similar shift in the fluorescence spectrum, as for the ECMP, is also observed for the closely related soluble pyrene SCMP material. Interpretation of spectra for SCMP is considerably more difficult because SCMP is a statistical copolymer of tetrafunctional and bifunctional units, and hence the material can contain fragments of tetrafunctional units linked to tetrafunctional units as well as bifunctional units linked to bifunctional units. The presence of the latter 'chains' could be an explantion to why the SCMP, in contrast, to ECMP is soluble in common organic solvents. The spectral similarities between both materials suggest that moderately strained 4- and 5-rings also exist in SCMP, and that they are the chromophore responsible for the SCMP fluorescence. The excess in fluorescence of SCMP relative to ECMP in the ∼450−480 nm range, coincident with the measured and predicted fluorescence maxima of the 1,3-linear pyrene polymer, might be the fingerprint of linear-chain rich, unbranched domains, that are absent, as discussed above, in the strictly alternating ECMP. The occurrence of this fluorescence excess also suggests that the chain-rich domains are large enough that at least some of the excitations originally generated there do not diffuse to more strained chromophores before radiative de-excitation to the ground state. Finally, a slight fluorescence excess at long wavelengths, at least for the precipitated SCMP sample (λ_{flu} > 550 nm) might also suggests the possible presence of SCMP-1 domains rich in tetrafunctional units (i.e., CMP-like domains).

On the basis of the above analysis, the absorption and fluorescence spectra of CMPs and related polymers should in principle be able to be engineered by the incorporation of different sizes of rings or rings with different degrees of strain. The ECMP and SCMP are examples of how expanding rings/reducing strain by incorporating bifunctional monomers allows one to blue shift the absorption and fluorescence spectra. This analysis is also in-line with the blue-shift observed between the pyrene CMP network and the ordered alternating 1:2 copolymer of tetrafunctional 1,3,6,8-tetrabromopyrene and bifunctional 1,4-benzene diboronic acid.[4] Copolymers with other ratios than 1:2 might yield intermediate blue-shifted spectra as long as the bifunctional monomer is homogenously

incorporated in the CMP. We have presented examples here for pyrene-based materials, but we believe that these general principles should hold for a much broader class of polymer network materials. Finally, a combination of the approach developed here with the Polymatic tool for building structural models of (amorphous) polymers[43] of Colina and co-workers could in the future lead to improved structural models of CMPs and related materials. Here the optical spectra of the material would be another constraint for the structural model to fulfill, just as the material's surface area, pore-volume etc.

CONCLUSIONS

A combination of theoretical and experimental spectroscopy provides an unrivalled insight into the atomic structure of porous conjugated polymers, where hitherto structures have been largely a matter of speculation and hypothesis. Specifically, we show that, in the case of an insoluble pyrene CMP network, the significant red shift in its absorption and fluorescence spectra relative to related pyrene-based materials can be rationalized by the presence of strained rings in a network structure. The incorporation of strained rings can, in principle, be exploited to tune the absorption and fluorescence spectra of a polymer, and hence optimize this for potential applications such as photocatalysis and photovoltaics. Certainly, these structural effects will be central in strategies which seek to control photophysical properties in porous organic polymers by "band gap engineering".[4]

ASSOCIATED CONTENT

Supporting Information

Full synthetic details, solution NMR spectra for soluble polymers and precursors, solid-state NMR spectra, FTIR spectra, UV−vis data, chemical composition data for the ECMP, further computational details regarding conformer searching, computational results for 1,8-oligomers, computational results on the thermodynamics of ring formation, computational results on the effect of strain in linear systems regarding ring structures, and discussion regarding excitation transfer in ring-based systems. This material is available free of charge via the Internet at http://pubs.acs.org.

AUTHOR INFORMATION

Corresponding Authors

*E-mail: (M.A.Z.) m.zwijnenburg@ucl.ac.uk.
*E-mail: (D.J.A.) d.j.adams@liverpool.ac.uk.

Present Addresses

[§]J.-X.J.: School of Materials Science & Engineering, Shaanxi Normal University, Xi'an P. R. China, 710062
[⊥]S.R.: College of Polymer Science and Engineering, Sichuan University, Chengdu, 610065, China

Author Contributions

The manuscript was written through contributions of all authors. All authors have given approval to the final version of the manuscript.

Notes

The authors declare no competing financial interest.

ACKNOWLEDGMENTS

M.A.Z. acknowledges the UK Engineering and Physical Sciences Research Council (EPSRC) for a Career Acceleration Fellowship (Grant EP/I004424/1). Computational time on HECToR the U.K.'s national high-performance computing service (via our membership of the UK's HPC Materials Chemistry Consortium, which is funded by EPSRC; Grants EP/F067496/1 and EP/L000202/1) and the EPSRC UK National Service for Computational Chemistry Software (NSCCS) at Imperial College London is gratefully acknowledged. We thank the EPSRC for funding (EP/H000925/1). A.I.C. is a Royal Society Wolfson award holder.

REFERENCES

(1) Jiang, J. X.; Su, F.; Trewin, A.; Wood, C. D.; Campbell, N. L.; Niu, H.; Dickinson, C.; Ganin, A. Y.; Rosseinsky, M. J.; Khimyak, Y. Z.; Cooper, A. I. *Angew. Chem., Int. Ed.* **2007**, *46*, 8574.
(2) Weber, J.; Thomas, A. *J. Am. Chem. Soc.* **2008**, *130*, 6334.
(3) Cooper, A. I. *Adv. Mater.* **2009**, *21*, 1291.
(4) Jiang, J. X.; Trewin, A.; Adams, D. J.; Cooper, A. I. *Chem. Sci.* **2011**, *2*, 1777.
(5) Kuhn, P.; Antonietti, M.; Thomas, A. *Angew. Chem., Int. Ed.* **2008**, *47*, 3450.
(6) Ren, S. J.; Bojdys, M. J.; Dawson, R.; Laybourn, A.; Khimyak, Y. Z.; Adams, D. J.; Cooper, A. I. *Adv. Mater.* **2012**, *24*, 2357.
(7) Ben, T.; Ren, H.; Ma, S. Q.; Cao, D. P.; Lan, J. H.; Jing, X. F.; Wang, W. C.; Xu, J.; Deng, F.; Simmons, J. M.; Qiu, S. L.; Zhu, G. S. *Angew. Chem., Int. Ed.* **2009**, *48*, 9457.
(8) Yuan, D. Q.; Lu, W. G.; Zhao, D.; Zhou, H. C. *Adv. Mater.* **2011**, *23*, 3723.
(9) Zhang, K.; Kopetzki, D.; Seeberger, P. H.; Antonietti, M.; Vilela, F. *Angew. Chem., Int. Ed.* **2013**, *52*, 1432.
(10) Chen, L.; Honsho, Y.; Seki, S.; Jiang, D. L. *J. Am. Chem. Soc.* **2010**, *132*, 6742.
(11) Kou, Y.; Xu, Y. H.; Guo, Z. Q.; Jiang, D. L. *Angew. Chem., Int. Ed.* **2011**, *50*, 8753.
(12) Vilela, F.; Zhang, K.; Antonietti, M. *Energy Environ. Sci.* **2012**, *5*, 7819.
(13) Jiang, J. X.; Trewin, A.; Su, F. B.; Wood, C. D.; Niu, H. J.; Jones, J. T. A.; Khimyak, Y. Z.; Cooper, A. I. *Macromolecules* **2009**, *42*, 2658.
(14) Trewin, A.; Cooper, A. I. *Angew. Chem., Int. Ed.* **2010**, *49*, 1533.
(15) Baerlocher, C.; McCusker, L. B.; Olson, D. H. *Atlas of Zeolite Framework Types*; 6th ed.; Elsevier: Amsterdam, 2007.
(16) O'Keeffe, M.; Hyde, B. G. *Crystal Structures - I. Patterns and Symmetry*; Mineralogical Society of America: Chantilly, VA, 1996.
(17) Zwijnenburg, M. A.; Illas, F.; Bromley, S. T. *Phys. Rev. Lett.* **2010**, 104.
(18) Abbott, L. J.; McDermott, A. G.; Del Regno, A.; Taylor, R. G. D.; Bezzu, C. G.; Msayib, K. J.; McKeown, N. B.; Siperstein, F. R.; Runt, J.; Colina, C. M. *J. Phys. Chem. B* **2013**, *117*, 355.
(19) Cheng, G.; Hasell, T.; Trewin, A.; Adams, D. J.; Cooper, A. I. *Angew. Chem., Int. Ed.* **2012**, *51*, 12727.
(20) Tian, J.; Thallapally, P. K.; Dalgarno, S. J.; McGrail, P. B.; Atwood, J. L. *Angew. Chem., Int. Ed.* **2009**, *48*, 5492.
(21) Jiang, S.; Jones, J. T. A.; Hasell, T.; Blythe, C. E.; Adams, D. J.; Trewin, A.; Cooper, A. I. *Nature Commun.* **2011**, *2*, 207.
(22) Hasell, T.; Chong, S. Y.; Jelfs, K. E.; Adams, D. J.; Cooper, A. I. *J. Am. Chem. Soc.* **2012**, *134*, 588.
(23) Brutschy, M.; Schneider, M. W.; Mastalerz, M.; Waldvogel, S. R. *Adv. Mater.* **2012**, *24*, 6049.
(24) Schneider, M. W.; Oppel, I. M.; Ott, H.; Lechner, L. G.; Hauswald, H. J. S.; Stoll, R.; Mastalerz, M. *Chem.—Eur. J.* **2012**, *18*, 836.
(25) Jorgensen, W. L.; Tiradorives, J. *J. Am. Chem. Soc.* **1988**, *110*, 1657.
(26) Kolossvary, I.; Guida, W. C. *J. Am. Chem. Soc.* **1996**, *118*, 5011.
(27) Furche, F.; Ahlrichs, R. *J. Chem. Phys.* **2002**, *117*, 7433.
(28) Furche, F.; Ahlrichs, R. *J. Chem. Phys.* **2004**, *121*, 12772.
(29) Yanai, T.; Tew, D. P.; Handy, N. C. *Chem. Phys. Lett.* **2004**, *393*, 51.
(30) Becke, A. D. *J. Chem. Phys.* **1993**, *98*, 5648.

(31) Valiev, M.; Bylaska, E. J.; Govind, N.; Kowalski, K.; Straatsma, T. P.; Van Dam, H. J. J.; Wang, D.; Nieplocha, J.; Apra, E.; Windus, T. L.; de Jong, W. *Comput. Phys. Commun.* **2010**, *181*, 1477.
(32) Schmidt, M. W.; Baldridge, K. K.; Boatz, J. A.; Elbert, S. T.; Gordon, M. S.; Jensen, J. H.; Koseki, S.; Matsunaga, N.; Nguyen, K. A.; Su, S. J.; Windus, T. L.; Dupuis, M.; Montgomery, J. A. *J. Comput. Chem.* **1993**, *14*, 1347.
(33) Hehre, W. J.; Ditchfie., R.; Pople, J. A. *J. Chem. Phys.* **1972**, *56*, 2257.
(34) van Wullen, C. *J. Comput. Chem.* **2011**, *32*, 1195.
(35) Ahlrichs, R.; Bar, M.; Haser, M.; Horn, H.; Kolmel, C. *Chem. Phys. Lett.* **1989**, *162*, 165.
(36) Schafer, A.; Horn, H.; Ahlrichs, R. *J. Chem. Phys.* **1992**, *97*, 2571.
(37) Figueira-Duarte, T. M.; Del Rosso, P. G.; Trattnig, R.; Sax, S.; List, E. J. W.; Mullen, K. *Adv. Mater.* **2010**, *22*, 990.
(38) Figueira-Duarte, T. M.; Simon, S. C.; Wagner, M.; Drtezhinin, S. I.; Zachariasse, K. A.; Mullen, K. *Angew. Chem., Int. Ed.* **2008**, *47*, 10175.
(39) Kawano, S. I.; Yang, C.; Ribas, M.; Baluschev, S.; Baumgarten, M.; Mullen, K. *Macromolecules* **2008**, *41*, 7933.
(40) Kasha, M. *Discuss. Faraday Soc.* **1950**, 14.
(41) Zwijnenburg, M. A. *J. Phys. Chem. C* **2012**, *116*, 20191.
(42) Zwijnenburg, M. A.; Bromley, S. T.; Foster, M. D.; Bell, R. G.; Delgado-Friedrichs, O.; Jansen, J. C.; Maschmeyer, T. *Chem. Mater.* **2004**, *16*, 3809.
(43) Abbott, L. J.; Hart, K. E.; Colina, C. M. *Theor. Chem. Acc.* **2013**, *132*, 1334.